

Improving electron beam quality in laser wakefield acceleration by using a plasma channel with an up-ramp density profile

Xin-Hui Wen(温昕辉), Xin-Zhe Zhu(祝昕哲), Mo Li(李墨), Jian Gao(高健), Bo-Yuan Li(李博原), Jian-Long Li(李建龙), Lin-Lu(鲁林), Ze-Wu Bi(毕择武), Wen-Chao Yan(闫文超), Feng Liu(刘峰), and Min Chen(陈民)
Citation: Chin. Phys. B, 2026, 35 (**6**): 065203. DOI: 10.1088/1674-1056/ae4b2f
http://cpb.iphy.ac.cn; http://iopscience.iop.org/cpb

What follows is a list of articles you may be interested in

Frequency chirp-induced enhancement of electron-positron pair production in polarized laser fields

Obulkasim Olugh(吾布力卡斯木·吾鲁克)
Chin. Phys. B, 2026, 35 (**4**): 045202. DOI: 10.1088/1674-1056/ae0a3c

Accelerating and guiding of electron beams in a cone target filled with near-critical-density plasmas

Jie-Jie Lan(蓝婕婕), Zhang-Hu Hu(胡章虎), and You-Nian Wang(王友年)
Chin. Phys. B, 2025, 34 (**12**): 125201. DOI: 10.1088/1674-1056/adea5b

Impact of mass concentration variations on plasma dynamics in a laser-ablated CH target

Hafiz Muhammad Siddique, Guannan Zheng(郑冠男), Tao Tao(陶弢), Xiao-Bao Jia(贾晓宝), and Jian Zheng(郑坚)
Chin. Phys. B, 2025, 34 (**11**): 115203. DOI: 10.1088/1674-1056/addcd0

Spectral characteristics of laser-plasma instabilities with a broadband laser

Guo-Xiao Xu(许国潇), Ning Kang(康宁), An-Le Lei(雷安乐), Hui-Ya Liu(刘会亚), Yao Zhao(赵耀), Shen-Lei Zhou(周申蕾), Hong-Hai An(安红海), Jun Xiong(熊俊), Rui-Rong Wang(王瑞荣), Zhi-Yong Xie(谢志勇), Xi-Chen Zhou(周熙晨), Zhi-Heng Fang(方智恒), and Wei Wang(王伟)
Chin. Phys. B, 2024, 33 (**8**): 085204. DOI: 10.1088/1674-1056/ad426d

Analysis of Landau damping in radially inhomogeneous plasma column

H Rajabalinia-Jelodar, M K Salem, F M Aghamir, H Zakeri-Khatir
Chin. Phys. B, 2018, 27 (**5**): 055203. DOI: 10.1088/1674-1056/27/5/055203

RAPID COMMUNICATION

Improving electron beam quality in laser wakefield acceleration by using a plasma channel with an up-ramp density profile

Xin-Hui Wen(温昕辉)[1,2], Xin-Zhe Zhu(祝昕哲)[1,2], Mo Li(李墨)[1], Jian Gao(高健)[1,2], Bo-Yuan Li(李博原)[1,2,†], Jian-Long Li(李建龙)[1,2], Lin Lu(鲁林)[1,2], Ze-Wu Bi(毕择武)[1,2], Wen-Chao Yan(闫文超)[1,2], Feng Liu(刘峰)[1,2], and Min Chen(陈民)[1,2,‡]

[1] *State Key Laboratory of Dark Matter Physics, Key Laboratory for Laser Plasmas (MOE), School of Physics and Astronomy, Shanghai Jiao Tong University, Shanghai* 200240, *China*

[2] *Collaborative Innovation Center of IFSA, Shanghai Jiao Tong University, Shanghai* 200240, *China*

(Received 26 January 2026; revised manuscript received 6 February 2026; accepted manuscript online 27 February 2026)

Laser wakefield acceleration (LWFA) is a promising way for producing GeV-scale electron beams within a tabletop size. Increasing acceleration energy and reducing energy spread are extremely important for many applications. Here, we experimentally demonstrate that using a plasma channel with a longitudinally up-ramp density profile can simultaneously boost the accelerated electron energy and lower the final beam energy spread. In a plasma channel with uniform plasma density, electron beams with a peak energy of 250 MeV and a large energy spread ($\sim 40\%$) were obtained. In contrast, within a plasma channel of the same length with an up-ramp density profile, stable electron beams with energies up to 1 GeV and a small energy spread ($\sim 20\%$) were observed. Particle-in-cell simulations show that the plasma channel not only suppresses laser diffraction, but also affects the self-injection and acceleration of the electron beam. In the up-ramp plasma channel, the continual electron injection is suppressed and electrons can be locked in the acceleration phase for a longer duration, which leads to the reduction of energy spread and the increase of electron energy. This method provides a relatively simple and reliable way toward compact, high-performance tabletop electron accelerators.

Keywords: laser plasma interactions, laser plasma wakefield acceleration, plasma waveguide

PACS: 52.38.–r, 41.75.Jv, 42.65.Wi

DOI: 10.1088/1674-1056/ae4b2f **CSTR:** 32038.14.CPB.ae4b2f

1. Introduction

The chirped pulse amplification (CPA) technique[1] has enabled ultra-intense, ultrashort lasers and spurred the rapid development of laser wakefield accelerators (LWFA),[2–4] which holds the potential to reduce the conventional kilometer-scale accelerators to a tabletop size.[5–7] LWFA can be broadly applied in medical imaging, materials science, and fundamental physics.[8–11] However, several challenges may restrict these applications: 1) the limited acceleration distance due to the natural laser diffraction and energy depletion;[12] 2) the limited acceleration energy due to the electron dephasing;[13] and 3) the not-so-good beam quality due to the uncontrolled electron injection.[14]

For the electron injection, self-injection is a simple way to trap electrons. It usually requires a relatively high laser intensity which can be obtained by tight laser focusing. However, the tight focusing also leads to fast laser diffraction and limited acceleration distance. To overcome the natural diffraction, plasma channels are usually employed, which can effectively guide the laser and increase the acceleration distance. However, achieving stable acceleration and high beam quality requires not only active control over laser guiding, but also precise management of both the phase of trapped electrons and their injection positions. Therefore, developing techniques for the active control of electron injection and acceleration length is crucial.[15–20]

In this paper, we use a plasma channel with an up-ramp density profile to simultaneously guide the laser pulse and control the electron injection and acceleration. Through experimental studies and three-dimensional particle-in-cell (PIC) simulations, we demonstrate that, compared with uniform-density conditions, the up-ramp density gradient can tune the laser evolution and modify the acceleration bubble size. These enable the electrons to be captured in the optimal acceleration phase. By this means, electron beams with a higher energy and a reduced energy spread are ultimately yielded.

2. Experimental setup and results

The experiment was conducted on the Chongming Laser-plasma Experimental Facility (CLEF) at Shanghai Jiao Tong University.[21] The laser pulse has a central wavelength of 800 nm, a pulse duration of 25 fs (FWHM), and an on-target energy of 3 J. The laser pulse was focused by an $f = 20$ off-

†Corresponding author. E-mail: liby1990@sjtu.edu.cn

‡Corresponding author. E-mail: minchen@sjtu.edu.cn

© 2026 Chinese Physical Society and IOP Publishing Ltd. All rights, including for text and data mining, AI training, and similar technologies, are reserved.

axis parabolic (OAP) mirror, yielding a focal spot of 26 μm (FWHM). A 3-cm-long, hollow-core quartz glass capillary with a 500 μm inner diameter is used to generate plasma channel.[22] Helium gas was filled from both ends of the capillary in a 50 ms duration and subsequently ionized by high-voltage discharge. In this way, an artificially controllable plasma channel can be produced to guide the laser pulse and motivate wakefield acceleration.[23] Electron energy is analyzed by a magnetic spectrometer composed by a dipole magnet with a field intensity of 1 T, a DRZ scintillator screen and a CCD camera. The experimental setup is shown in Fig. 1.

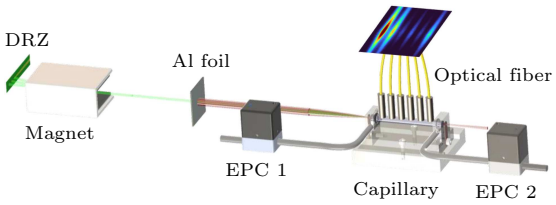


Fig. 1. Schematic of the experimental setup. A 3-cm-long capillary is mounted on a holder, filled with helium gas, and then is discharged to form a plasma channel. Two electronic pressure controllers (EPCs) are used at both ends of the capillary to control the gas pressure independently, allowing the creation of a longitudinally tailored density profile. The optical fibers are used to collect the discharge light for the diagnosis of plasma density. A thin aluminum foil placed behind the capillary blocks the residual laser light. The electron beam, which transmits through the foil, is then analyzed by a magnetic spectrometer.

To control the electron injection and acceleration process, the capillary was connected to two independent gas inlets at its two ends, which enabled the separate control of back pressure through each solenoid valve. After high-voltage discharging, the helium gas inside the capillary was ionized to a plasma state. To measure the axial plasma density profile, six optical fibers were used to collect the discharge light signal, which was subsequently delivered to an imaging spectrometer to analyze the plasma density by calibrating the spectral broadening [Fig. 2(a)].

The plasma density was determined from the Stark broadening of the helium-β line ($\lambda = 587.6$ nm). By analyzing the spectral broadening of each optical fiber, the local plasma density at each position was deduced. The Stark broadening formula for the helium-β line is

$$\lg(n_e) = a + b \times \left(\sqrt{\frac{T_e}{T_c}} + \sqrt{\frac{T_c}{T_e}} + \sqrt{\frac{T_e}{T_m \mu}} \right) + p \lg(\Delta\lambda).$$

In the formula, T_e represents the plasma electron temperature, and $\Delta\lambda$ is the full width at half maximum of the broadened line. The remaining terms are constants. As found in the literature,[24,25] the values are $a = 23.2871$, $b = 0.08306$, $p = 0.98894$, $T_c = 11648$, $T_m = 132390$. By substituting the measured $\Delta\lambda$ for each fiber into the formula, the local plasma density n_e can be calculated.

In our experiments, under a back pressure of 2.1 bar, a plasma density of 1.6×10^{18} cm^{-3} can be measured around the corresponding gas inlets. By reducing the back pressure at the laser entrance, a plasma channel with a longitudinally up-ramped density profile can be constructed. As shown in Fig. 2(b), by using the same gas-inflation back pressure, the plasma density along the capillary axis is uniform. When we changed the entrance back pressure to 1.8 bar, a typical linear up-ramp density profile from 1.4×10^{18} cm^{-3} to 1.6×10^{18} cm^{-3} can be obtained.

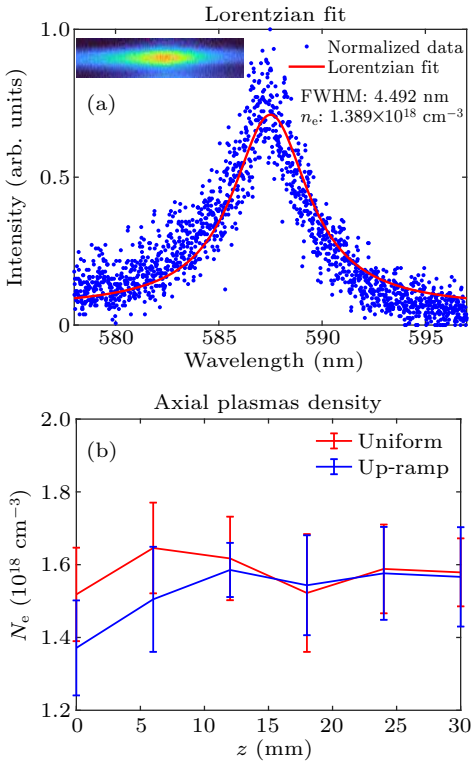


Fig. 2. Typical spectral broadening of helium-587.6 nm characteristic line (a) and the deduced axial plasma density profile of the discharged capillary (b). The spectral broadening is determined by the full width at half maximum of the Lorentzian fitting. In (b), each data point representing an average over 10 consecutive shots.

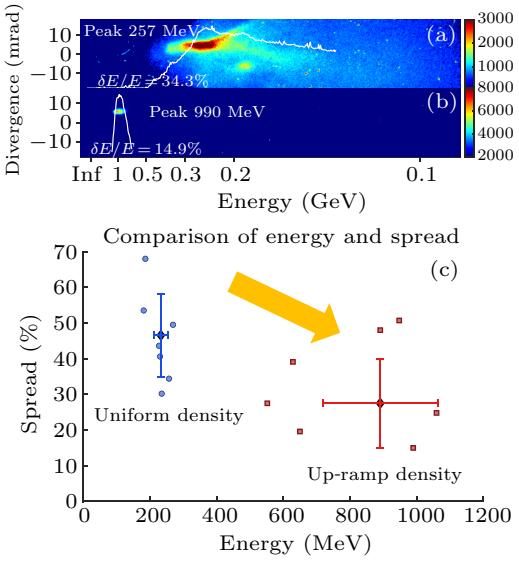


Fig. 3. Comparison of electron spectra under different axial plasma density profiles. (a) Uniform density profile. (b) Up-ramp density profile. (c) Statistical results of the central energy and energy spread of electron beams.

Figure 3 shows two typical electron energy spectra accelerated from plasma channels with a uniform density profile [Fig. 3(a)] and an up-ramp density profile [Fig. 3(b)]. As one can see, the spectrum in the uniform density case shows a broad energy spectrum and a peak energy around 250 MeV. In contrast, in the up-ramp density case, the spectrum exhibits a sharp quasi-monoenergetic peak centered around 0.99 GeV and the relative energy spread ($\Delta E/E$) is reduced to 14.9%. More statistical results are shown in Fig. 3(c). It clearly confirms that by using an up-ramp density profile, the maximum electron energy can be remarkably increased and the energy spread can be reduced. In the next section, we will explain the underlying physical mechanism through particle-in-cell simulations.

3. Particle-in-cell simulations and mechanism analysis

To analyze the reason for the improvement of the electron beam quality, three-dimensional simulations using the Fourier–Bessel particle-in-cell (FBPIC) code were performed.[26] The simulated laser parameters are similar to the experimental conditions. The normalized amplitude of the laser pulse is $a_0 = eE_0/(m\omega c) = 1.7$, the pulse duration is 25 fs, and the focal spot radius is 25.5 μm. Along the laser propagation direction, a plasma channel whose depth matches the laser radius is used to reproduce the experimental conditions. The total simulation length is 35 mm, with the plasma channel in the central 30 mm section. Two density profiles were implemented for comparison: a uniform profile with a density of 1.6×10^{18} cm^{-3} (uniform case), and an up-ramp profile with a density increasing from 1.4×10^{18} cm^{-3} to 1.6×10^{18} cm^{-3} (up-ramp case). The numerical setup employed open boundary conditions in both longitudinal (z) and radial (r) directions, and a moving window (velocity $v_{\text{window}} = 0.999c$) to follow the laser propagation. The plasma-vacuum transitions at the channel entrance and exit were smoothly modeled with linear axial ramps over 2.5 mm and gradual radial transitions over 100 μm. Key simulation parameters are listed as follows: azimuthal modes $N_{\text{m}} = 2$, solver order $n_{\text{order}} = 32$, particle initialization with $p_{nz} = 2$, $p_{nr} = 2$, $p_{nt} = 8$ per cell, grid dimensions $N_z = 3200$, $N_r = 600$ corresponding to resolutions $\Delta z = 50$ nm and $\Delta r = 0.2$ μm, and time step $\Delta t = \Delta z/c = 1.67 \times 10^{-16}$ s.

We first study the electron injection process in the two cases. Simulations reveal that using a plasma channel allows the laser to propagate over a long distance without diffraction while undergoing a nonlinear self-focusing effect, which raises its normalized amplitude (a_0) at specific positions and then results in electron self-injection under the nonlinear wakefield. The details of such processes are shown in Fig. 4. Figures 4(a) and 4(d) show the evolutions of laser intensities and the injection positions for the two cases. The corresponding wake bubble and electron energy spectrum at the beginning and end moments of the injection process are shown in the second and third rows in Fig. 4. For the uniform-density case, the electron self-injection occurs earlier due to the initial plasma density being higher than that in the up-ramp case. During this stage, a large number of electrons are continuously trapped over an extended injection period, leading to a broad energy spread. However, for the up-ramp density case, due to the initial low density, the onset of laser self-focusing and electron injection are both delayed. The effective injection region is shorter, which leads to a lower energy spread.

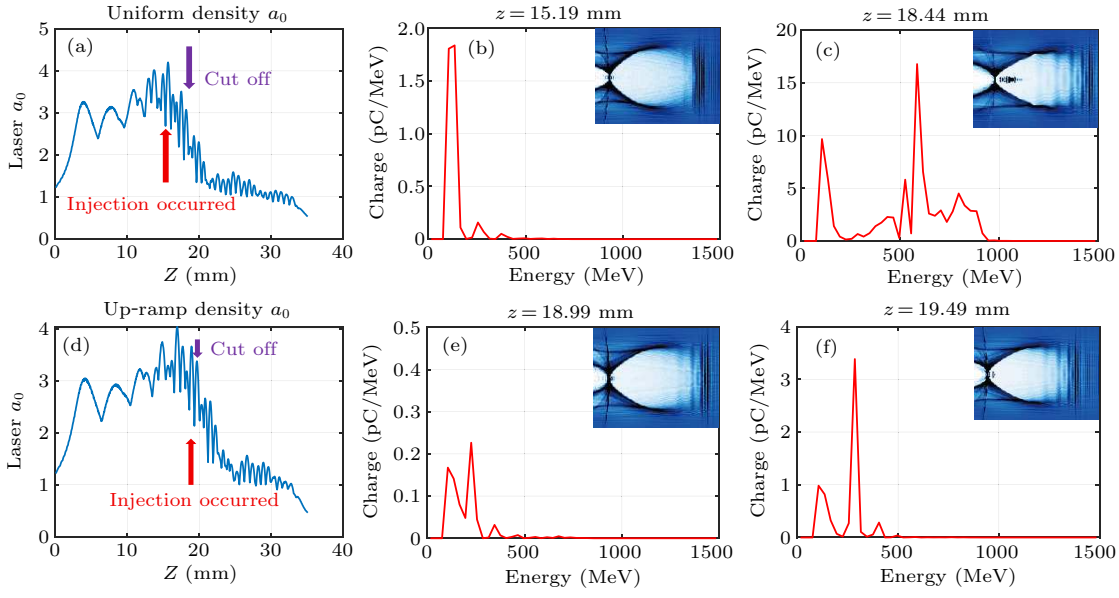


Fig. 4. Differences in electron injection and acceleration for the two cases. Panels (a) and (b)–(c) show the evolution of the normalized laser amplitude a_0 and the electron energy spectrum (with the electron position inside the bubble presented in the insets)at the injection trigger point and injection cut-off point, respectively, for the uniform density case. Panels (d)–(f) display the corresponding results for the up-ramp density case.

Self-injection usually occurs when the longitudinal velocity of background electrons is larger than the phase velocity of wake fields. Both the laser intensity (a_0) and the local plasma density can affect the size of the wake bubble, thereby influencing the phase velocity of wake fields. The bubble size depends on the plasma density n_e and the laser's normalized amplitude a_0 as $r \propto \sqrt{a_0}/\sqrt{n_e}$.[27–29] In the uniform density case, the bubble size mainly depends on the laser intensity which periodically increases to cause the bubble expansion and reduce the wake phase velocity, finally triggering the electron injection. The sustained focusing leads to the continuous injection, which produces a large energy spread of the electron bunch. However, in the up-ramp plasma channel, the bubble size tends to decrease as the plasma density rises, which exerts a significant counteracting effect on the electron self-injection. The self-injection depends on the local balance of the laser self-focusing and the increase of plasma density, which is quite sensitive and only lasts for a short region. This leads to a reduction of electron energy spread. As shown in Fig. 4, in the entire simulation, the injection process only takes place between the points labeled "injection occurred" and "cut off". For the uniform case, injection started at 15.19 mm and ended at 18.44 mm, lasting for 2.75 mm. However, for the up-ramp case, injection was delayed to the position at 18.99 mm and ended at 19.49 mm, only lasting for 0.5 mm.

After being injected into the wake bubble, electrons gain energy in the acceleration phase. The final energy gain depends on the acceleration stage. In the plasma, the wakefield phase velocity may remain subluminal. As the electron velocity approaches the speed of light, electrons gradually move towards the head of the wake bubble. Eventually, they enter the deceleration phase — a process known as dephasing. The dephasing length in a longitudinally uniform density plasma is given by $l_{\mathrm{dephasing}} = \frac{2\sqrt{a_0}}{3\pi}\frac{\lambda_p^3}{\lambda_1^2}$,[30–32] which is typically on the order of millimeters to centimeters. Therefore, in long plasma channels of several centimeters, electron dephasing is a common effect that limits the maximum energy. In the experiment, it is observed that the fluctuations in peak energy are larger in the channel with an up-ramp density profile compared with the channel with a uniform density profile [Fig. 3(c)]. This is because the fluctuation of the gas-filling in the density up-ramp channel is larger, thereby affecting the acceleration length. In the uniform channel case, all electrons are eventually dephased, resulting in smaller energy fluctuations.

From the simulations, we see that in a uniform channel, the injected electrons are continuously accelerated at the beginning, with the maximum energy even approaching ~ 1 GeV (but with large energy spread) as shown in Fig. 5(a). However, in the latter part of the channel, the electrons enter the deceleration phase and steadily lose energy as shown in Fig. 5(b). Finally, the mean energy of the electron bunch is reduced to about 500 MeV when exiting the plasma channel [Fig. 5(c)]. By contrast, in the up-ramp density channel, the injected electrons always remain in the acceleration phase, as shown in Fig. 5(e). This allows continuous acceleration until the exit of the plasma channel, achieving a final energy gain of 1 GeV [Fig. 5(f)]. It should be noted that even if the uniform channel is truncated before the electrons enter the deceleration phase, the energy spread of the resulting GeV electron beam is still larger than that produced in the up-ramp channel. Therefore, the up-ramp density channel offers a distinct advantage over the truncated uniform channel for obtaining a high-quality electron beam.

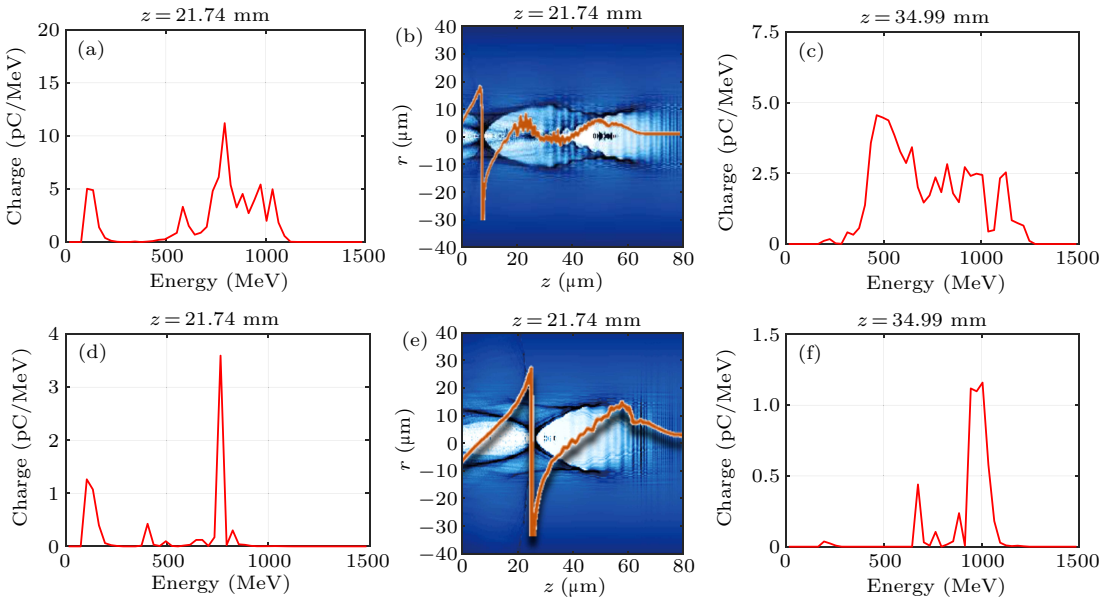


Fig. 5. (a) Simulated electron energy spectrum at $z = 21.74$ mm in the uniform channel. (b) Electron beam location inside the plasma bubble corresponding to (a) and the on-axis electric field profile. (c) Final electron energy spectrum after passing through the entire uniform channel. (d)–(f) The corresponding results for the case using plasma channel with up-ramp density profile.

4. Conclusion

In summary, our study shows that the up-ramp plasma channel could improve the electron beam quality compared to the uniform plasma channel. First, during the injection stage, it can cut off the self-injection faster, resulting in a low-energy-spread electron bunch. Second, in the acceleration stage, the density increase effectively maintains the phase-locking of the electron beam, achieving higher energy gain in a long plasma channel. These advantages finally lead to a significant increase in the electron energy and a reduction in the energy spread.

Acknowledgements

This work was supported by the National Natural Science Foundation of China (Grant Nos. 12225505 and 11991074), Shanghai Jiao Tong University 2030 Initiative, Fundamental and Interdisciplinary Disciplines Breakthrough Plan of the Ministry of Education of China (Grant No. JYB2025XDXM204), the Strategic Priority Research Program of the Chinese Academy of Sciences (Grant No. XDB0530303), the National Key Research and Development Program of China (Grant No. 2021YFA1601700), and Al for Science Program, Shanghai Municipal Commission of Economy and Informatization (Grant No. 2025-GZL-RGZN-BTBX-02029). The simulations were performed at the π Supercomputer Center at SJTU.

References

[1] Strickland D and Mourou G 1985 *Opt. Commun.* **56** 219
[2] Tajima T and Dawson J M 1979 *Phys. Rev. Lett.* **43** 267
[3] Esarey E, Schroeder C B and Leemans W P 2009 *Rev. Mod. Phys.* **81** 1229
[4] Chen M, Liu F, Li B Y, Weng S M, Chen L M, Sheng Z M and Zhang J 2020 *High Power Laser Part. Beams* **32** 092001
[5] Faure J, Glinec Y, Pukhov A, Kiselev S, Gordienko S, Lefebvre E, Rousseau J P, Burgy F and Malka A 2004 *Nature* **431** 541
[6] Mangles S P D, Murphy C D, Najmudin Z, Thomas A G R, Collier J L, Dangor A E, Divall E J, Foster P S, Gallacher J G, Hooker C J, Jaroszynski D A, Langley A J, Mori W B, Norreys P A, Tsung F S, Viskup R, Walton B R and Krushelnick K 2004 *Nature* **431** 535
[7] Geddes C G R, Toth C, Tilborg J V, Esarey E, Schroeder C B, Bruhwiler D, Nieter C, Cary J and Leemans W P 2004 *Nature* **431** 538
[8] Corde S, Phuoc T K, Lambert G, Fitour R, Malka V, Rousse A, Beck A and Lefebvre E 2013 *Rev. Mod. Phys.* **85** 1
[9] Zhu X Z, Li B Y, Liu F, Li J L, Bi Z W, Ge X L, Deng H Y, Zhang Z Y, Cui P L, Lu L, Yan W C, Yuan X H, Chen L M, Cao Q, Liu Z Y, Sheng Z M, Chen M and Zhang J 2023 *Phys. Rev. Lett.* **130** 215001
[10] Mourou G A, Tajima T and Bulanov S V 2006 *Rev. Mod. Phys.* **78** 309
[11] Wang W T, Feng K, Ke L T, *et al.* 2021 *Nature* **595** 516
[12] Miao B, Feder L, Shrock J E, Goffin A and Milchberg H M 2020 *Phys. Rev. Lett.* **125** 074801
[13] Rittershofer W, Schroeder C B, Esarey E, Grüner F J and Leemans W P 2010 *Phys. Plasmas* **17** 063104
[14] Picksley A, Stackhouse J, Benedetti C, Nakamura K, Tsai H E, Li R, Miao B, Shrock J E, Rockafellow E, Milchberg H M, Schroeder C B, Tilborg J V, Esarey E, Geddes C G R and Gonsalves A J 2024 *Phys. Rev. Lett.* **133** 255001
[15] Gonsalves A J, Nakamura K, Daniels J, *et al.* 2019 *Phys. Rev. Lett.* **122** 084801
[16] Volfbeyn P, Esarey E and Leemans W P 1999 *Phys. Plasmas* **6** 2269
[17] Gaul E W, Blanc S P L, Rundquist A R, Zgadzaj R, Langhoff H and Downer M C 2000 *Appl. Phys. Lett.* **77** 4112
[18] Chen M, Esarey E, Schroeder C B, Geddes C G R and Leemans W P 2012 *Phys. Plasmas* **19** 1229
[19] Ke L T, Feng K, Wang W T, Qin Z Y, Yu C H, Wu Y, Chen Y, Qi R, Zhang Z J, Xu Y, Yang X J, Leng Y X, Liu J S, Li R X and Xu Z Z 2021 *Phys. Rev. Lett.* **126** 214801
[20] Chen M, Sheng Z M, Ma Y Y and Zhang J 2006 *J. Appl. Phys* **99** 056109
[21] Gao J, Li B Y, Yan W C, Liu F, Chen M. J. 2026 *High Power Laser and Part. Beams* **38** 031003
[22] Li J L, Li B Y, Zhu X Z, Bi Z W, Wen X H, Lu L, Yuan X H, Liu F and Chen M 2023 *High Power Laser Sci. Eng.* **11** e58
[23] Zhu X Z, Li B Y, Liu F, Li J L, Bi Z W, Lu L, Yuan X H, Yan W C, Chen M, Chen L M, Sheng Z M and Zhang J 2022 *Acta Phys. Sin.* **71** 095202 (in Chinese)
[24] Nikiforov A Y, Leys C, Gonzalez M A and Walsh J L 2015 *Plasma Sources Sci. Technol.* **24** 034001
[25] Griem H R, Baranger M, Kolb A C and Oertel G 1962 *Phys. Rev.* **125** 177
[26] Rémi L, Manuel K, Igor A A, Brendan B G and Jean L V 2016 *Comput. Phys. Commun.* **203** 66
[27] Pukhov A and Meyer T V J 2002 *Appl. Phys. B* **74** 355
[28] Pukhov A, Gordienko S, Kiselev S and Kostyukov I 2004 Plasma Phys. Controlled Fusion **46** B179
[29] Kostyukov I, Pukhov A and Kiselev S 2004 *Phys. Plasmas* **11** 5256
[30] Palastro J P, Shaw J L, Franke P, Ramsey D, Simpson T T and Froula D H 2020 *Phys. Rev. Lett.* **124** 134802
[31] Pukhov A and Kostyukov I 2008 *Phys. Rev. E* **77** 025401
[32] Guillaume E, Döpp A, Thaury C, Phuoc K T, Lifschitz A, Grittani G, Goddet J P, Tafzi A, Chou S W, Veisz L and Malka V 2015 *Phys. Rev. Lett.* **115** 155002